Journal of Materials Chemistry C

PAPER

View Article Online
View Journal

Cite this: DOI: 10.1039/c4tc01134a

Electrochemical deposition as a unique solution processing method for insoluble organic optoelectronic materials†

Emily Allwright,[a] Dominik M. Berg,[b] Rabie Djemour,[b] Marc Steichen,[b] Phillip J. Dale[b] and Neil Robertson*[a]

Received 30th May 2014
Accepted 11th July 2014

DOI: 10.1039/c4tc01134a

www.rsc.org/MaterialsC

Electrochemical deposition is shown to be a novel technique to deposit films of *N*,*N*′-dibutylperylene-3,4:9,10-bis(dicarboximide) (BuPTCDI) dye that avoids the need for high vacuum or solubilising side chains on the molecule. The technique exploits the higher solubility of the reduced ionic form of the dye over the neutral form. BuPTCDI was chemically reduced to solubilise and then electrochemically oxidised to form a film on various substrates. The properties of the films were investigated by UV/Vis spectroscopy, Photoluminescence, Raman spectroscopy, X-ray diffraction, SEM and photoconductivity showing the successful deposition of the BuPTCDI molecules. The technique was also used to deposit films on interdigitated-electrode substrates enabling measurement of field-effect mobility.

Introduction

Research into the deposition of organic thin films for optoelectronic applications has resulted in the development of several methods of fabrication,[1] mainly divided into two types: solution deposition and vapour deposition. Solution deposition techniques such as spin coating[2,3] and dip coating[4] have been used to deposit repeatable, uniform thin films on a small scale. Larger scale production methods undergoing research include screen printing,[5] spray deposition[6] and ink jet printing.[7,8] These techniques however, rely on the deposited material being soluble. To achieve effective charge transport, organic semiconductor materials are designed to have a large degree of intermolecular interaction which most of the time is obtained by large π-stacked systems. This often results in the parent molecule being insoluble, requiring addition of solubilising substituents such as alkyl chains. It may be difficult to deposit good quality films of these materials by solution techniques and the films produced inevitably contain insulating alkyl domains that affect the desired semiconducting properties. Vapour techniques are also used to produce thin films; the advantage of this method is to allow fabrication of high quality thin films of well controlled thickness and the fabrication of complex multi-layered architectures.[9] This technique however, also has disadvantages as a commercially viable option for large area depositions as it requires vacuum and is generally time consuming.[10] Another problem relates to the temperature required, as large π-stacked systems normally have high sublimation points and many will decompose before subliming. Compounding this, very high substrate temperatures may be needed to achieve good crystallinity.[11]

Electrochemical deposition has the potential to be used as an alternative method for depositing insoluble molecules onto conductive substrates. This method works by chemically changing the redox state of a molecule to solubilise it, then electrochemically changing it back to its insoluble form at a conducting substrate. For extended-lattice materials, the electrochemical deposition of inorganic semiconductor thin films has emerged as an alternative to vapour deposition techniques over the past decade.[12–15] In contrast however, electrodeposition of small molecules for use in molecular electronics has received almost no attention. An early study used an electrode formed from the neutral compound. This was partly dissolved on reduction and then oxidised onto a titanium dioxide slide.[16] The technique showed promise in the deposition of thin films but has not received subsequent attention.[17] More recently, we have shown, in the case of metal-bis-1,2-dithiolene complexes, that the deposition of the neutral molecules onto field-effect transistor (FET) substrates and fluorine doped tin oxide (FTO) conducting glass was successfully achieved from the dissolved molecular anions using potentiostatic electrodeposition.[18,19] The films deposited using this method were found to be polycrystalline, with higher conductivity than films deposited by solvent casting. Dithiolene complexes provided a convenient test case to explore the electrodeposition method due to both the neutral and anionic states being readily isolated and stable

[a]School of Chemistry and EaStCHEM Research School, University of Edinburgh, King's Buildings, West Mains Road, Edinburgh, EH9 3JJ, UK. E-mail: neil.robertson@ed.ac.uk
[b]Université du Luxembourg, Laboratory for Energy Materials, 41 rue du Brill, L-4422 Belvaux, Luxembourg

† Electronic supplementary information (ESI) available: Fig S1: Raman spectra, optical picture of film, UV/Vis of re-dissolved film; Fig. S2 XRD single crystals and film comparison; Fig. S3 additional FET data. See DOI: 10.1039/c4tc01134a

in air. This feature however, is not commonly shared by molecules used in organic electronics. This has prompted us to further develop the technique and we report here a general approach to the electrodeposition method that should be broadly applicable to all small molecules suitable for organic optoelectronic materials. This may prove particularly relevant for molecules unsuitable for solution processing or vapour processing due to their poor solubility or poor thermal stability respectively.

To establish our new methodology, we have studied perylene-3,4,9,10-bis(dicarboximide) (PTCDI) dyes, which have attracted interest due to their organic, electronic and optical properties.[20] In this paper we have studied the electrodeposition of *N*,*N*′-dibutylperylene-3,4,9,10-bis(dicarboximide) (*BuPTCDI*) and the properties of the resulting films. Most significantly, we present a general experimental approach to film processing that may be applied to any molecule under study for organic electronic materials, and suggest this as a novel processing route, complementary to typical solution or vapour deposition.

Experimental

All solvents used were dried and purified by passage through activated alumina columns using a solvent purification system. Chemicals used were purchased from Aldrich. The perylene diimide derivative, BuPTCDI, was prepared by the condensation of perylenetetracarboxylic dianhydride with *n*-butylamine as previously described by Schnurpfeil.[21] UV-Vis (THF): $\lambda_{max} = 270$, 357, 445, 475, 512 560 nm. CHN: cal: C 76.5%, H 5.2%, N 5.6% found: C 76.7%, H 5.6%, N 5.7%.

Electrodeposition

Sodium (*ca.* 200 mg, 8.7 mmol) was removed from the storage oil and placed in a test tube under N_2. The sodium was washed three times with degassed THF to remove any trace of the storage oil. The sodium was then evaporated to form a sodium mirror. BuPTCDI (44 mg, 0.087 mmol) suspended in dry degassed THF (3 ml) was added to the sodium and stirred under N_2 for *ca.* 240 min. The solution was then filtered into an electrochemical cell containing a solution of dry degassed acetonitrile (10 ml) containing 0.1 M $TBABF_4$ electrolyte. Film deposition was performed using a modified three electrode setup. FTO coated glass was used as the working electrode, a Pt pseudo reference electrode calibrated against ferrocene/ferrocenium was used with a standard Pt counter electrode. The latter was separated from the other electrodes by a porous glass frit. Electrochemistry experiments were performed using an Autolab type III potentiostat using GPES software. Electrochemical data are quoted against ferrocene/ferrocenium.

X-ray diffraction of the film was performed on a Bruker Discover D8 with a Cu $K_{\alpha 1}$ source and a scintillation detector. Raman spectra were recorded using a Horiba Labram HR high resolution spectrometer equipped with a mulitchannel detection system in the backscattering configuration. Solution emission spectra were recordeded at 77 K using a Fluoromax2 fluorometer controlled by ISAmain Software. The film excitation was performed using an Ar ion laser (514 nm). Photoelectrochemical measurements were performed by chopping a standard halogen cold mirror lamp with nominal light intensity of 100 mW cm^{-2}. Photocurrents were recorded using a three-electrode setup with a platinum wire counter electrode and a Ag/AgCl reference electrode in 0.1 M KCl aqueous solution with hydroquinone (0.1 M), a sacrificial electron donor. The film was treated with a napthol polymer to fill any holes present. To ensure that the film was not rendered completely passive the amount of current required to cover a third of the film's area was calculated. The film was then treated several times to make sure that the pores present were completely filled. Once the photocurrent response stopped increasing and started decreasing it suggested that the pores were full and that napthol was depositing on the film's surface. Field-effect transistor measurements were performed by electrochemically depositing BuPTCDI onto interdigitated-electrode substrates, consisting of a silicon wafer gate electrode with a SiO_2 layer as the insulating layer. Platinum source and drain electrodes were deposited onto the insulating layer with an electrode gap of 8 μm. Current–voltage measurements were recorded using a Keithley 2612A source probe measuring the drain current (I_{SD}) as a function of the applied source drain voltage (V_{SD}) at various applied gate voltages (V_{SG}).

SEM images were obtained using Philips XL30CP with PGT Spirit X-ray analysis and HKL Channel5 Electron Backscatter Diffraction (EBSD) systems. The specification of the instrument is a tungsten filament source electron gun and the resolution of the microscope is 3.5 nm at 30 kV using the secondary electron (SE) detector.

Results and discussion

Film deposition

Cyclic voltammetry performed on the neutral BuPTCDI molecule in THF, in which it shows slight solubility, revealed two reversible reductions at $E_{1/2} = -1.04$ V and $E_{1/2} = -1.36$ V (Fig. 1 inset). This is consistent with literature values of other PTCDI cores as the carbonyl groups allow for the formation of a stable

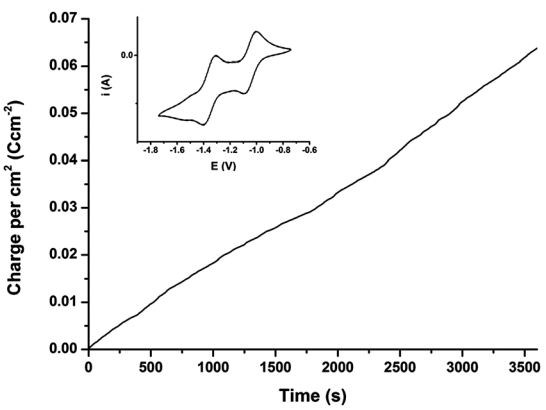

Fig. 1 Total charge per cm^2 passed during a 60 minute (3600 s) deposition holding the voltage at 0.30 V. Inset: cyclic voltammogram of BuPTCDI between −1.0 and 0 V in 0.1 M $TBABF_4$ in THF.

anion and dianion at reduction voltages depending on the specific groups present in the imide positions.[22] After preparing the solution of Na_x[BuPTCDI] as described in the Experimental section, the films were deposited by holding the working electrode at a constant voltage of 0.3 V for a set amount of time. The potential was chosen to give a reasonable rate of deposition without being sufficiently positive to damage the film, which was observed for example at +1.0 V. The steady current indicates that the film is sufficiently conducting to continue to enable further film growth on the deposited material. The exact stoichiometry of the reduction process is not known with the possibility of mono or dianionic BuPTCDI. The resulting films on FTO, prepared using different deposition times, were rinsed with acetonitrile and left in air to dry.

Raman spectroscopy of the deposited films was carried out and the resulting spectra (Fig S1, Table S1†) were compared with spectra of perylene-diimide thin films studied by Rodríguez-Llorente *et al.* to identify the main peaks of the BuPTCDI.[23] The peaks observed confirm that the thin film is composed of BuPTCDI showing similar proprieties to the film deposited by thermal evaporation. Furthermore, re-dissolution of the deposited film in excess THF showed the UV/Vis spectrum to be the same as that of the starting BuPTCDI (Fig. S1†). No evidence of any decomposition of the molecules was therefore observed during the electrodeposition process.

SEM imaging and thickness determination

Images of the films' surface and cross sections were obtained by scanning electron microscopy (SEM) which showed that the films contained various sizes of crystallites rather than a homogeneous flat surface (Fig. 2), and that the majority of the larger elongated crystallites appeared to grow perpendicular to the surface. This suggests that the material growth occurs preferentially upon BuPTCDI seed points rather than the bare FTO surface, such that micron scale film thickness is required before continuous film coverage is achieved. An SEM image of the cross section (Fig. 3) further shows that there are little or no crystallite structures parallel to the FTO surface, with most at angles greater than 45°.

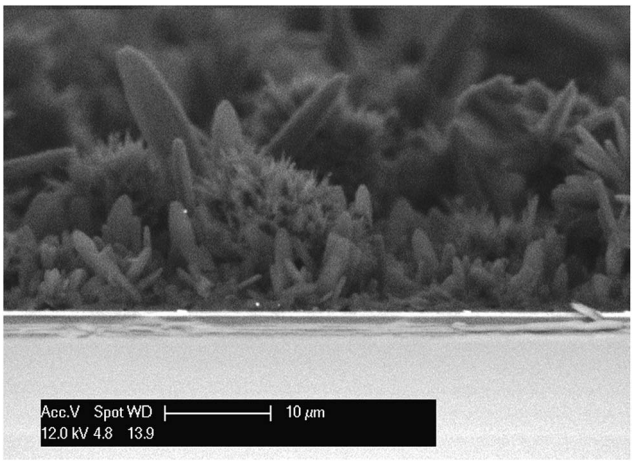

Fig. 3 SEM image of an electrodeposited BuPTCDI film cross-section (3600 s).

Elongated crystal growth perpendicular to the substrate is consistent with the electrochemical mechanism, with preferred growth, consistent with higher conductivity, along the needle axis. This can be attributed to cofacially stacked perylene cores with π-stacking in the perpendicular direction,[24] resulting in columnar stacks.[25]

The thicknesses of the films were determined by snapping the FTO substrate and analysing the cross-section of the film *via* SEM. Since the films were rough due to crystallite formation, an average thickness was estimated along with a minimum and maximum height. A plot of the average thickness, with minimum and maximum film thickness shown as vertical bars, against the charge per cm^2 passed during the electrochemical deposition is shown in Fig. 4.

As would be expected, the average thickness, as well as the range for the maximum and minimum thickness, increased with the amount of charge passed during deposition. By comparing the observed thickness with the charge passed per

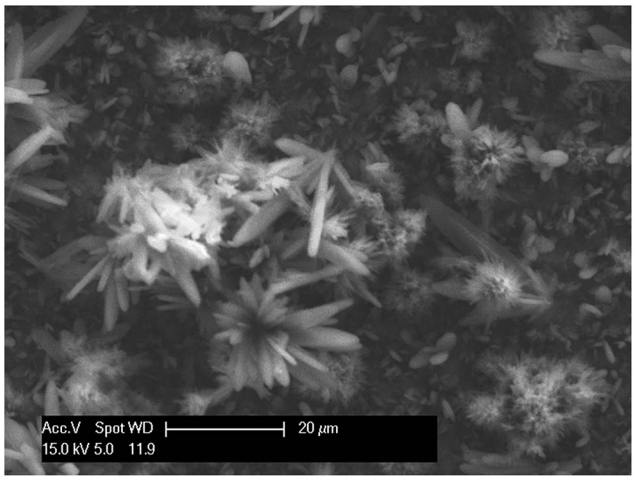

Fig. 2 SEM image of a BuPTCDI film surface on FTO after deposition (3600 s).

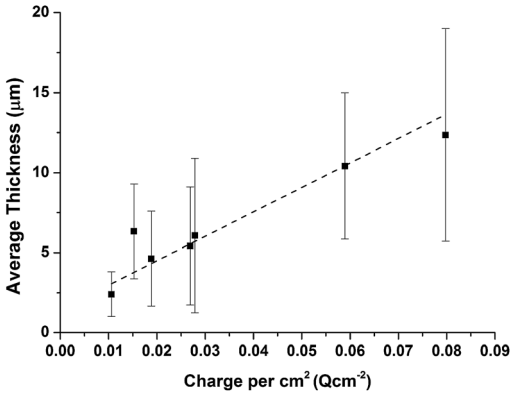

Fig. 4 Average film thickness *versus* charge per cm^2 passed. The bars represent maximum and minimum thicknesses observed across the film.

cm^2 it is possible to estimate the charge per cm^2 needed to produce a film of a determined thickness. A line of best fit applied to Fig. 4 gave the formula:

$$\text{Thickness(observed)}/\mu\text{m} = (153 \pm 18) \times \text{Charge}/(\text{C cm}^{-2})$$

Based on the crystal structure and assuming a one-electron redox process, the charge required to give a particular thickness of a dense film is described by the following formula:

$$\text{Thickness(theory)}/\mu\text{m} = (36.6) \times \text{Charge}/(\text{C cm}^{-2})$$

This indicates that the electrodeposited films are ~4 times thicker than would be expected from theory (or 8 time thicker for a two-electron redox process) for a dense single-crystal film with zero porosity. This is consistent with Fig. 2 and 3 which show that the electrodeposited film is not a uniform compact crystal and possess considerable unfilled volume. Although not possible to directly calculate, this also suggests that the electrodeposition is reasonably efficient with the reductive current leading to deposited film without excessive material being lost.

X-ray diffraction

The X-ray diffraction pattern of an electrodeposited BuPTCDI film on FTO was recorded and is shown in Fig. 5 below. Using Bragg's Law the *d*-spacings corresponding to the observed peaks were calculated (Table 1). The peaks present were compared to the simulated powder patterns of the two known single-crystal polymorphs obtained by Graser[26] and Mizuguchi[27] respectively, as well as XRD patterns of PTCDIs films deposited by other techniques found in literature. The cell dimensions of the two known single crystal structure are displayed in Table 2.

The XRD pattern of the film suggests a combination of two types of crystalline material. Two strong sharp peaks dwarf several broader peaks, suggesting that the films are made up of very crystalline structures as well as less crystalline material. This agrees with the cross-section SEM image in Fig. 3 where there is a combination of needle-like crystallites and smaller clusters of material. Additionally however, the dominance of the two peaks with *d*-spacings of 11.9 Å and 11.6 Å may suggest some preferred orientation within the more crystalline material.

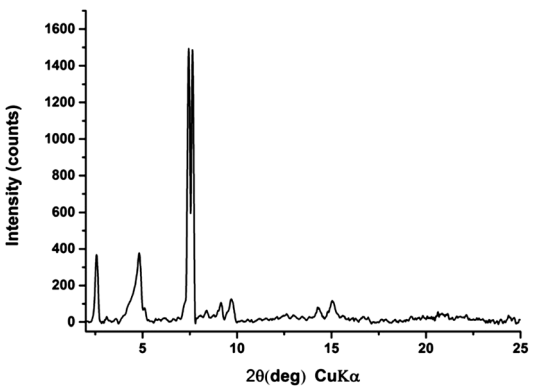

Fig. 5 XRD pattern of an electrodeposited BuPTCDI film.

Table 1 Calculation of *d*-spacings

BuPTCDI Film 2θ values	BuPTCDI Film *d* values (Å)
2.56	34.48
4.8	18.39
7.43	11.89
7.61	11.61
9.14	9.67
9.7	9.11
14.31	6.18
15.05	5.88

The electrodeposited film pattern shows that the packing of the molecules in the film is different to both known single crystal structures (Fig. S2†). It also does not show close similarities with thin-film structures of related RPCDTI molecules prepared by vapour deposition.[24,25] In both known crystal structures of BuPTCDI the perylene forms a herringbone-type packing with the smallest dimension for both structures being the π–π stacking of the cores at about 4.6 Å. Our film data however, do not enable resolution of a corresponding Bragg peak that would be expected at high angle.

For the electrodeposited film, the largest *d*-spacings, 34.2 Å and 18.2 Å are probably cell lengths, broadly comparable with one of the literature structures (Table 2) although with the longest axis somewhat longer, perhaps suggesting a smaller tilt angle of the BuPTCDI stacks compared with the herringbone packing seen by Graser and Mizuguchi.

Absorption spectroscopy

The solution UV/Vis absorbance of BuPTCDI in different solvents was measured and compared with the spectrum of the electrodeposited film (Fig. 6).

Perylene complexes in solution have a characteristic absorption between 445 nm and 520 nm and this is clearly observed in the two solution spectra. In addition, there is also the development of a shoulder in the DMSO spectrum, attributed to the π–π interactions of the molecules due to aggregation. The films of BuPTCDI clearly display absorbance across a similar spectral region consistent with the deposition of BuPTCDI molecules. The considerable band broadening is attributed to molecular packing leading to significant intermolecular interactions as would be expected in the solid state. This is accompanied by a red shift of the low energy absorption

Table 2 Cell dimensions of the two known crystal structures of BuPTCDI (Å)

	Graser[26] (Å)	Mizuguchi[27] (Å)
a	4.73	18.41
b	28.23	4.63
c	9.40	27.61

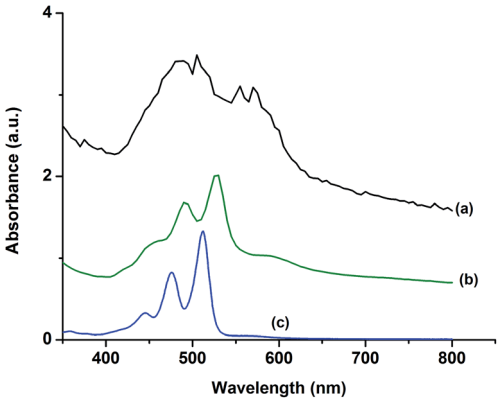

Fig. 6 UV/Vis spectra of BuPTCDI (a) electrodeposited on FTO, (b) dissolved in DMSO and (c) dissolved in THF.

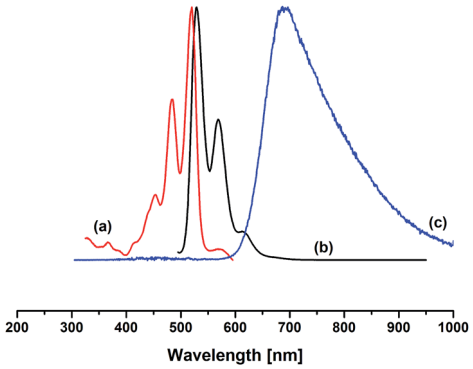

Fig. 8 Photoluminescence of BuPTCDI: (a) excitation spectrum in THF (monitored at 614 nm) (b) emission spectrum in THF (excited at 475 nm) (c) emission of an electrodeposited BuPTCDI film (excited at 514 nm).

onset compared to the spectra of the BuPTCDI in solution consistent with greater electron delocalisation from the intermolecular π-stacking.[28] Such absorption characteristics due to π–π interactions are important for organic electronics and agree with data of films deposited by vapour deposition.[29]

Comparing different depositions, we observe a general trend relating the absorbance and the quantity of material deposited (Fig. 7), with higher absorbance resulting from increased charge passed per cm^2. Numerical correlation between absorbance and charge passed was not possible however due to the significant scattering observed in many of the films that made accurate absorbance values not possible to determine. Some example films where scattering was less dominant are shown in Fig. 7.

Photoluminescence

The photoluminescent response of BuPTCDI was measured in solution and in an electrochemically deposited film (Fig. 8). BuPTCDI in solution shows fluorescence with emission maxima at 454, 485 and 520 nm. The proximity of the two peaks and the near mirror symmetry of the absorption and emission spectra suggest that there is little distortion in the configuration of the molecule when it is excited from the ground state to the excited state.[30] The emission spectrum of the film shows a very different response to the isolated molecule in solution. The spectrum of the film is a broad featureless band with a maximum around 679 nm, due to the excimers in the perylene film[28,31] and typical also of other thin solid films.[32] Again these results are consistent with deposition of intact perylene molecules showing considerable intermolecular interaction in the film.

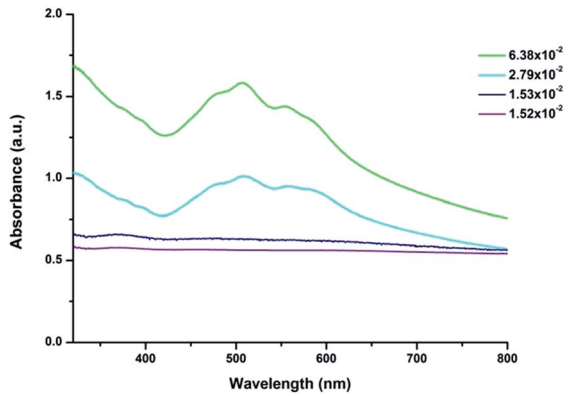

Fig. 7 Absorbance of several different films deposited with differing total charge passed (Ccm^{-2}, indicated by the inset) showing increased absorbance for the thicker films.

Charge mobility and photoconductivity

The electrodeposition technique was also used to grow films of BuPTCDI on interdigitated-electrode substrates suitable for study of field-effect transistor (FET) properties. The charge transport characteristics of several different PTCDI compounds have previously been studied[24,33–36] and have shown that most PTCDIs show electron transporting properties. In previous work on vapour-deposited BuPTCDI, the measured current has shown a typical field-effect response with a range of μFET from 4×10^{-6} cm^2 V^{-1} s^{-1} to 0.6 cm^2 V^{-1} s^{-1}.[35,36]

Films were deposited directly onto platinum-electrode substrates and were then held at a constant voltage of 0 V until they showed no more signs of decharging. In order to observe a field-effect of the conductivity, it is essential to minimise any doping that may remain from the deposition process which would result in a high off-current and holding the films at a low voltage ensured that the films were not charged. Field-effect measurements were carried out on a freshly deposited BuPTCDI film on interdigitated platinum-electrode substrates (Fig. 9).

Fig. 9 shows the current measured between the source and drain electrodes as a function of the applied source–drain voltage for increasing source–gate voltages. The currents measured show a stepwise increase in current with the increased source–gate voltage, indicating that the applied source–gate voltage is affecting the flow of electrons in the deposited film. The current measured is also typical of bulk transport of electrons with a large off-current, which is likely due to the relative thickness of the film. These observations agree with the SEM images which suggest that the crystals grow perpendicular to the substrate, hence complete coverage of the

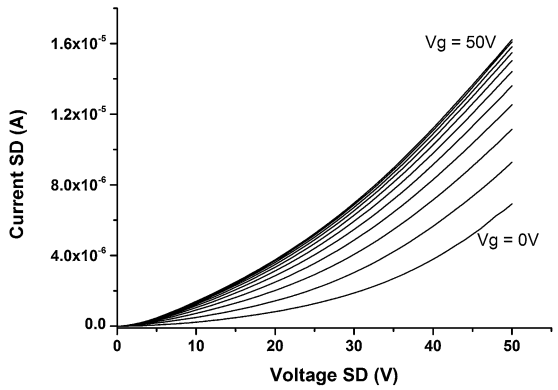

Fig. 9 Drain current *vs.* source–drain voltage curves at various source–gate voltages for BuPTCDI field effect transistors.

gaps in the interdigitated electrode requires a thick film. The observed mobility is also expected to be low due to the undesirable orientation of the long crystallite axes perpendicular to the source–drain direction.

Extraction of an accurate mobility from the data is somewhat compromised by the large off-current, however an estimate can be made. Applying a linear fit to the current, the calculated electron mobility of the material is $\mu FET = 2.3 \times 10^{-8}$ cm^2 V^{-1} s^{-1}. This is lower than previously-reported field-effect mobilities measured for perylenediimide molecules, although this is as expected for the reasons described above. The current measured decreases over time, which suggests that there is some degradation in the device (Fig. S3†). This is consistent with previous studies of related molecules, in which the field-effect disappeared due to degradation between the FET substrate and the deposited film.[34]

To further probe the electronic properties of the films, photoelectrochemical studies were performed by monitoring the electrochemical response of the film on FTO under chopped illumination by a halogen light at 100 mW cm^{-2}. To minimise any effect at the bare electrode, the film was treated with naphthol to fill any holes between the BuPCDTI crystallites. The response is plotted in Fig. 10 and shows an increase in current when the film is exposed to light and a subsequent decrease when the light is off. The photocurrent response of the untreated film shows a significant off-current, contrasting with the naphthol-treated film where the off-current is suppressed (Fig. 10). This indicates that the untreated films are porous enough for the electrolyte to directly interact with the FTO substrate irrespective of illumination. These observations are consistent with the crystalline, rather than continuous nature of the films shown by SEM (Fig. 2 and 3). The photoelectrochemical response again illustrates in general the formation of a light-absorbing BuPTCDI film able to transport charge.

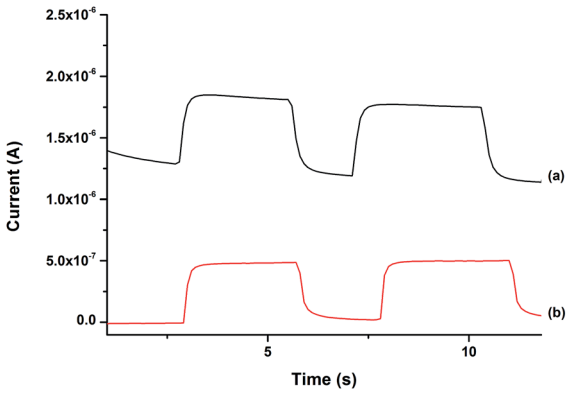

Fig. 10 Current against time response at 0.1 V to a chopped halogen lamp showing higher current with light on: (a) untreated film and (b) naphthol-treated film.

Conclusions

Electrochemical deposition has been developed as a novel technique for the formation of *N*,*N*′-dibutylperylene-3,4,9,10-bis(dicarboximide) films. The chemical reduction of the PTCDIs to enable dissolution, followed by the electrochemical oxidation onto FTO substrates offers a unique method of deposition as an alternative to other solution and vapour processing techniques.

Several methods were applied to the deposited films to analyse their optical and electronic properties and to compare them to the powder form of the molecule and to films deposited by other techniques. Raman and UV/Vis absorption spectroscopy confirmed that the electrodeposited films include the intact molecules, with similar properties to thin films deposited by other techniques. SEM imaging and X-ray diffraction showed the morphology of the film was polycrystalline and included elongated crystallites perpendicular to the FTO substrate. This perpendicular growth is likely the result of the stacked perylene π-cores giving higher conductivity, hence a preferential growth direction perpendicular to the substrate. A plot of average thickness against charge per cm^2 enables prediction of film thickness, controlled by the amount of current passed. The electronic properties of the films measured on electrodeposited field effect transistors showed bulk electron transport and evidence of controlled doping *via* application of a potential at the gate electrode. On FTO, the films showed visible-light photoconductivity.

Although the material properties of the BuPTCDI film are not optimised for device function, in particular due to the crystalline rather than continuous nature, the key demonstration of this work is a novel approach to film deposition in organic (opto)electronic materials. The electrodeposition method may in principle be applied to any electroactive molecule, offering a solution-processing route for insoluble or involatile materials, without the need for extensive alkyl substitutents to achieve high solubility and without the need for thermal stability to enable vapour processing. In particular, we see opportunities for this method as a complementary approach where the established deposition techniques are not suitable. For example, electrodeposition may be used to deposit organic materials on non-planar surfaces such as mesoporous solids, and further work is ongoing to explore other molecules, substrates and devices.

Acknowledgements

We thank Fonds National de Luxembourg for a studentship for EA.

Notes and references

1 (*a*) F. C. Krebs, *Sol. Energy Mater. Sol. Cells*, 2009, **93**, 394–412; (*b*) Y. Wen, Y. Liu, Y. Guo, G. Yu and W. Hu, *Chem. Rev.*, 2011, **111**, 3358; (*c*) A. C. Arias, J. D. MacKenzie, I. McCulloch, J. Rivnay and A. Salleo, *Chem. Rev.*, 2010, **110**, 3.

2 Y. Lin, P. Cheng, Y. Liu, X. Zhao, D. Li, J. Tan, W. Hu, Y. Li and X. Zhan, *Sol. Energy Mater. Sol. Cells*, 2012, **99**, 301–307.

3 H. Shang, H. Fan, Q. Shi, S. Li, Y. Li and X. Zhan, *Sol. Energy Mater. Sol. Cells*, 2010, **94**, 457–464.

4 Z. Hu, J. Zhang, S. Xiong and Y. Zhao, *Sol. Energy Mater. Sol. Cells*, 2012, **99**, 221–225.

5 S. E. Shaheen, R. Radspinner, N. Peyghambarian and G. E. Jabbour, *Appl. Phys. Lett.*, 2001, **79**, 2996–2998.

6 N. A. Azarova, J. W. Owen, C. A. McLellan, M. A. Grimminger, E. K. Chapman, J. E. Anthony and O. D. Jurchescu, *Org. Electron.*, 2010, **11**, 1960–1965.

7 C. N. Hoth, S. A. Choulis, P. Schilinsky and C. J. Brabec, *Adv. Mater.*, 2007, **19**, 3973–3978.

8 F. C. Krebs, M. Jørgensen, K. Norrman, O. Hagemann, J. Alstrup, T. D. Nielsen, J. Fyenbo, K. Larsen and J. Kristensen, *Sol. Energy Mater. Sol. Cells*, 2009, **93**, 422–441.

9 B. Kippelen and J.-L. Bredas, *Energy Environ. Sci.*, 2009, **2**, 251–261.

10 J. K. Kim, W. Kim, D. H. Wang, H. Lee, S. M. Cho, D.-G. Choi and J. H. Park, *Langmuir*, 2013, **29**, 5377–5382.

11 D. B. Mitzi, *Adv. Mater.*, 2009, **21**, 3141–3158.

12 W. E. Buschmann, S. C. Paulson, C. M. Wynn, M. A. Girtu, A. J. Epstein, H. S. White and J. S. Miller, *Chem. Mater.*, 1998, **10**, 1386–1395.

13 D. Lincot, *Thin Solid Films*, 2005, **487**, 40–48.

14 C. J. Hibberd, E. Chassaing, W. Liu, D. B. Mitzi, D. Lincot and A. N. Tiwari, *Prog. Photovoltaics*, 2010, **18**, 434–452.

15 A. P. Samantilleke, M. Sahal, L. Ortiz, M. F. Cerqueira and B. Marí, *Thin Solid Films*, 2011, **519**, 7272–7275.

16 A. Zaban and Y. Diamant, *J. Phys. Chem. B*, 2000, **104**, 10043–10046.

17 Y. Diamant and A. Zaban, *J. Electrochem. Soc.*, 2001, **148**, C709–C714.

18 S. Dalgleish, H. Yoshikawa, M. M. Matsushita, K. Awaga and N. Robertson, *Chem. Sci.*, 2010, **2**, 316–320.

19 S. Dalgleish, K. Awaga and N. Robertson, *Chem. Commun.*, 2011, **47**, 7089–7091.

20 F. Gao, Y. Zhao and W. Liang, in *The Journal of PhysicalChemistry B*, American Chemical Society, 2011, pp. 2699–2708.

21 G. Schnurpfeil, J. Stark and D. Wöhrle, *Dyes Pigm.*, 1995, **27**, 339–350.

22 G. Türkmen, S. Erten-Ela and S. Icli, *Dyes Pigm.*, 2009, **83**, 297–303.

23 S. Rodríguez-Llorente, R. Aroca and J. Duff, *Spectrochim. Acta, Part A*, 1999, **55**, 969–978.

24 R. J. Chesterfield, J. C. McKeen, C. R. Newman, C. D. Frisbie, P. C. Ewbank, K. R. Mann and L. L. Miller, *J. Appl. Phys.*, 2004, **95**, 6396–6405.

25 C. W. Struijk, A. B. Sieval, J. E. J. Dakhorst, M. van Dijk, P. Kimkes, R. B. M. Koehorst, H. Donker, T. J. Schaafsma, S. J. Picken, A. M. van de Craats, J. M. Warman, H. Zuilhof and E. J. R. Sudhölter, *J. Am. Chem. Soc.*, 2000, **122**, 11057–11066.

26 E. Hadicke and F. Graser, *Acta Crystallogr., Sect. C: Cryst. Struct. Commun.*, 1986, **42**, 189–195.

27 J. Mizuguchi, *Z. Kristallogr. New Cryst. Struct.*, 2003, 131–133.

28 V. Parra, T. Del Cano, M. L. Rodriguez-Mendez, J. A. de Saja and R. F. Aroca, *Chem. Mater.*, 2003, **16**, 358–364.

29 J. Mizuguchi, *Dyes Pigm.*, 2006, **70**, 226–231.

30 T. Kircher and H. G. Lohmannsroben, *Phys. Chem. Chem. Phys.*, 1999, **1**, 3987–3992.

31 D. Schlettwein, A. Back, B. Schilling, T. Fritz and N. R. Armstrong, *Chem. Mater.*, 1998, **10**, 601–612.

32 W. Yip and D. H. Levy, *J. Phys. Chem.*, 1996, **100**, 11539–11545.

33 R. J. Chesterfield, J. C. McKeen, C. R. Newman, P. C. Ewbank, D. t. A. da Silva Filho, J.-L. BrÃ©das, L. L. Miller, K. R. Mann and C. D. Frisbie, *J. Phys. Chem. B*, 2004, **108**, 19281–19292.

34 G. Horowitz, F. Kouki, P. Spearman, D. Fichou, C. Nogues, X. Pan and F. Garnier, *Adv. Mater.*, 1996, **8**, 242–245.

35 D. Lehmann and D. R. T. Zahn, *Appl. Phys. A: Mater. Sci. Process.*, 2009, **95**, 203–207.

36 P. R. L. Malenfant, C. D. Dimitrakopoulos, J. D. Gelorme, L. L. Kosbar, T. O. Graham, A. Curioni and W. Andreoni, *Appl. Phys. Lett.*, 2002, **80**, 2517–2519.